KINETIC ENERGY OF FRAGMENTS FROM THE PHOTOFISSION OF U^{238}

B. A. BOCHAGOV, A. P. KOMAR, and G. E. SOLYAKIN

Leningrad Physico-Technical Institute, Academy of Sciences, U.S.S.R.

A double ionization chamber was employed to study the energy distribution of U^{238} photo-fission fragments. Gamma rays with $E_{\gamma\,max}$ = 70 Mev were produced by the synchrotron of the Physico-Technical Institute. A topological plot of the fragment kinetic energy distribution is compared with diagrams representing the fission of heavy elements induced by neutrons of various energies.

INTRODUCTION

THE photofission of heavy nuclei has not yet been investigated with sufficient thoroughness. Most of the literature (see reference 1, for example) has been concerned with a) fission cross sections, b) the number of neutrons per fission event, c) the mass distribution of fragments, and d) the correlation between the directions of fragments and the gamma-ray beam.

Only two papers have appeared on the energy distribution of fragments,[2,3] which is important both for the understanding of the fission mechanism and for reactor technology.[4] The data presented in references 2 and 3 were obtained by means of pulse ionization chambers with electron collection. The apparatus was able to register the energy of only one fragment per fission. We believe it is extremely important to determine the energy distribution of fragments as completely as in the case of neutron-induced fission.[5-8] A comparison of the distributions for photofission and for neutron-induced fission could be very important for the further development of fission theory.

The present paper reports some results obtained by our laboratory during 1955 in investigations of the photofission of heavy nuclei, particularly U^{238}.

EXPERIMENTAL PROCEDURE

For the measurement of photofission fragment energies we used two pulse ionization chambers with electron collection (Fig. 1). The target material was deposited on the common high-voltage electrode 5 of the chambers, which are more fully described in references 5, 6 and 13. Figure 1 is a block diagram of our apparatus. Voltage pulses
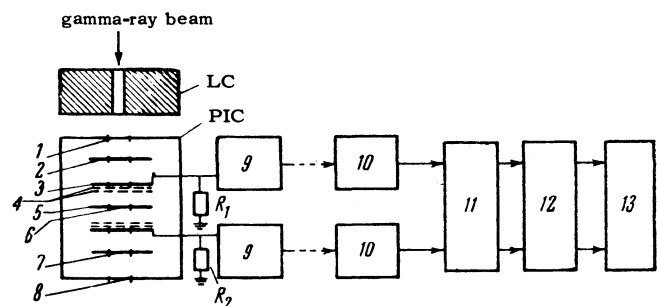
gamma-ray beam

FIG. 1. Block diagram of apparatus. LC – lead collimator, PIC – pulse ionization chamber, 1 – ionization chamber entrance window, 2 – compensating electrode, 3 – collecting electrode, 4 – screening grids, 5 – common high-voltage electrode, 6 – Zapon film bearing layer of uranyl nitrate, 7 – aperture for passage of gamma-ray beam (present in all electrodes); (the second half of the chamber is a mirror image of the first half); 8 – exit window, R_1 and R_2 – resistors from which voltage pulses are taken, 9 – preamplifiers, 10 – main amplifiers, 11 – time gate, 12 – control circuit of loop oscillograph, 13 – MPO-2 loop oscillograph.

from the resistors R were amplified by the preamplifiers 10 and were then fed to the time gate 11, which blocked the amplifier outputs except when gamma rays were passing through the chambers; this was done in order to obviate electrical induction produced by the synchrotron. Pulses passing through the time gate and control circuit 12 reached the MPO-2 loop oscillograph 13 for motion-picture recording. The ionization-chamber electrodes were positioned perpendicular to the direction of the gamma-ray beam.

The synchrotron of the Physico-Technical Institute of the USSR Academy of Sciences provided a gamma-ray beam with $E_{\gamma max}$ = 70 Mev, which was defined by a lead collimator LC. Compensating electrodes in the ionization chambers served to compensate pulses induced by the gamma radiation. Compensation was facilitated by

increasing the duration of gamma-ray pulses from 10 to 1500 μsec. The maximum gamma-ray energy of 70 Mev was selected to produce a greater intensity in the giant resonance region, since photofission is known to result mainly from the absorption of photons in this energy region.

The target was a layer of uranyl nitrate, containing a natural mixture of uranium isotopes, which was deposited on a Zapon film fastened in a brass ring of 40 mm inside diameter. A thin layer of aluminum deposited on each side made the film an electrical conductor; its thickness including the aluminum was 30 μg/cm^2. The thickness and uniformity of the uranyl nitrate layer were determined from the alpha-particle spectrum of natural uranium. The spectrum registered on the uranyl nitrate side is shown in Fig. 2; the spectrum registered on the film side does not differ essentially. The thickness of the uranyl nitrate deposit was 320 μg/cm^2. The alpha-particle energy peaks were used as reference values in determining the fission fragment energies.
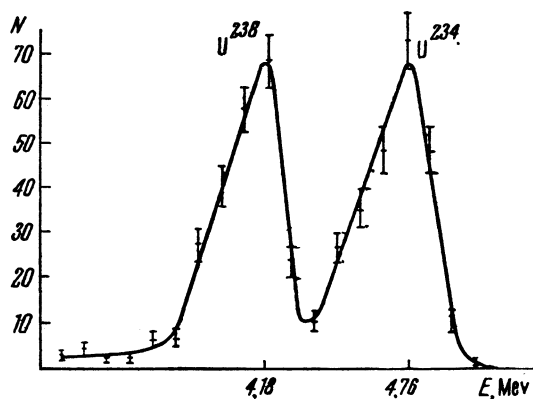

FIG. 2. Alpha-particle spectrum of natural uranium registered on the uranyl nitrate side of the target.

Chuvilo[9] found that all detected fragments from a natural uranium target result, to within 1%, from the fission of U^{238}. The film-recorded amplitudes V_1 and V_2 of heavy and light fragments were proportional to the number of ion pairs produced by each fragment in the chamber, i.e., they were proportional to the kinetic energies E_1 and E_2 of the fragments. We have assumed that the energy required to produce an ion pair is identical for fragments and alpha particles. We measured the pulse heights on a flat projection obtained by means of a photographic enlarger.

Thus each fission event was associated with two numerical values E_1 and E_2; the indices 1 and 2 pertain to the chambers (chamber 1 was closer to the synchrotron target). Figure 3 shows $W_{ik} = n_{ik}/n_{ik\,max}$, the distribution (in
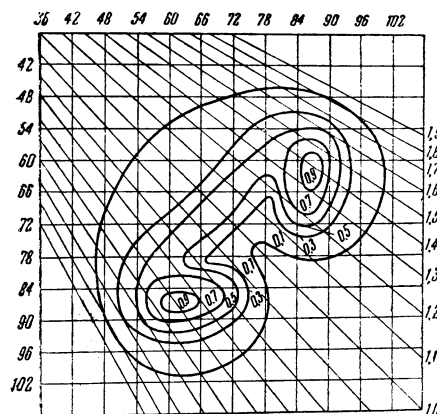

FIG. 3. Topological plot — contour lines of the surface $W_{ik}(E_1, E_2)$. The coordinates represent the energies E_1 and E_2 of the two fragments in Mev.

relative units) of the numbers of cases n_{ik} of different pairs of values for E_1 and E_2. Corrections for energy losses in the target amounted to 5%. Figure 3 also shows lines representing E_1/E_2 = const. All results are given without corrections for source thickness and the ionization defect. Errors in the positions of the maxima in the graphs equal half of the interval width used in plotting.

RESULTS AND DISCUSSION

The contour lines of the surface W_{ik} were plotted in Fig. 3 for intervals $\Delta W_{ik} = 0.2$, thus revealing only the most general features of the surface. However, detailed topological information is very important for the understanding of the fission mechanism. Because of the discreteness of the data we studied slices of W_{ik} of finite width in different directions. We found it most useful to consider slices formed by planes parallel to the coordinate planes, perpendicular to the principal diagonal and to the XY plane, and by planes perpendicular to the XY plane and intersecting the latter along lines of constant E_1/E_2. We were interested in the dependence of n_{ik} and $N = \Sigma n_{ik}$ on E_1 and E_2, i.e., on the local topology and "mass" of the slices. We shall show that the type of slice and N are determined by the limitations imposed on i and k.

The main characteristic of the surface $W_{ik}(E_1, E_2)$ is its mirror symmetry with respect to the vertical plane through the principal diagonal ($E_1 = E_2$). This symmetry denotes that either a heavy or a light fragment is ejected in a given direction with equal probability.

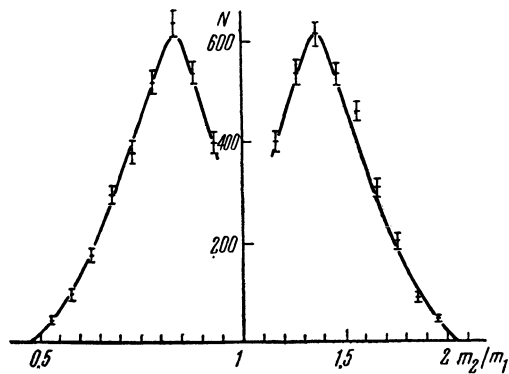Any asymmetry of these fragments would easily be detected in Fig. 4, which represents

FIG. 4. Photofission fragment yield of U^{238} as a function of the mass ratio $m_2/m_1 = E_1/E_2$.

the total number of cases in slices of type Δ (E_1/E_2) as a function of E_1/E_2. Figure 3 shows that the most probable fragment energies are 87 and 61 Mev, while Fig. 4 indicates that the most probable mass ratio is 1.36. Thus the ratio of the most probable masses, $m_2/m_1 = E_1/E_2 = 1.43$, does not equal the most probable mass ratio. Similar discrepancies are found in the neutron-induced fission of U^{235} and U^{238}.[5,6]

If it is assumed that a U^{238} nucleus loses two neutrons in each photofission event, the most probable light and heavy fragment masses will be 100 and 136, thus agreeing, within the limits of error, with radiochemical results for U^{238}.[10]

A second important characteristic of W_{ik} is the presence of two pronounced symmetrical hills having ridge lines parallel to the coordinate axes. This indicates constancy of the most probable energies E_l and E_h, of light and heavy fragments for different intervals ΔE_1 and ΔE_2.

Similar hills have been found on the corresponding surfaces for the neutron-induced fission of U^{235}, U^{233}, Pu^{239} and Pu^{241},[5-8] and for the spontaneous fission of Cf^{252}.[11] In these cases the median lines of the ridges were curves whose tangents formed small angles with the coordinate axes. Figure 3 clearly shows that when $E_1/E_2 = m_2/m_1 = const$ there is considerable spread of the combined fragment energy $\Sigma E = E_1 + E_2$ and a smaller spread of the most probable values of this energy. Figure 5 shows the number of instances n_{ik} as a function of ΣE for different slices between adjacent planes $E_1/E_2 = const$. Between $E_1/E_2 = 1.2$ and $E_1/E_2 = 1.1$ the curves exhibit two peaks. For larger values of E_1/E_2 the most probable value of the combined energy, corresponding to the left-hand peak in Fig. 5, is reduced. For $E_1/E_2 = 1.5$ to 1.4 this peak becomes a barely perceptible step, and for E_1/E_2
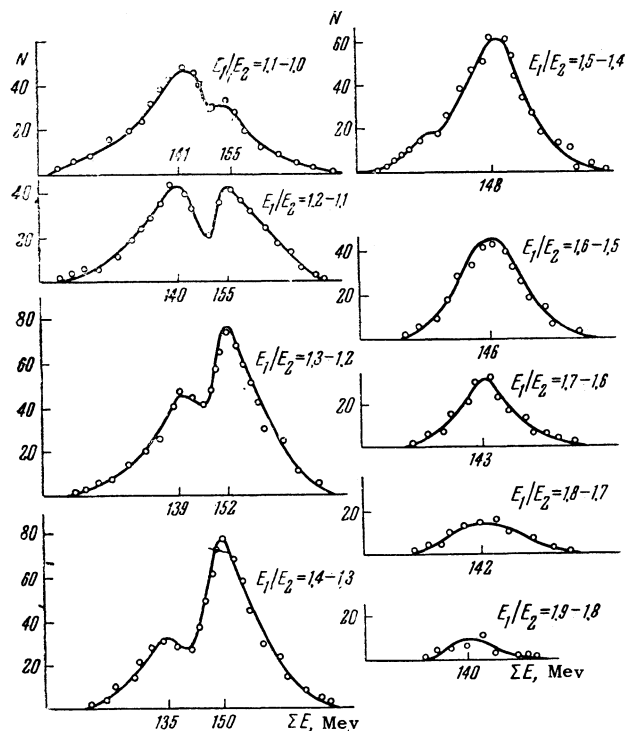

FIG. 5. Total fragment (kinetic) energy $\Sigma E = E_1 + E_2$ in U^{238} photofission for different mass ratios E_1/E_2.
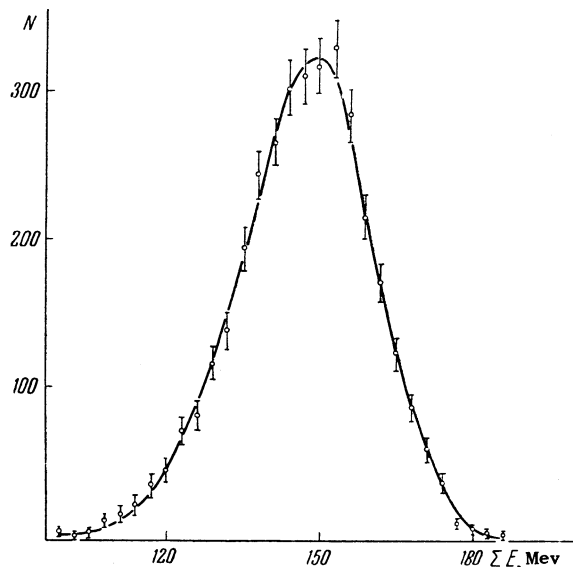
= 1.6 to 1.5 it disappears completely. The right-hand peak, which is just noticeable for $E_1/E_2 = 1.1$ to 1.0, is gradually transformed into the only peak with the change of E_1/E_2 from 1.6 — 1.5 to 1.9 — 1.8.

Wahl[12] has observed a similar characteristic of the combined-energy distribution for U^{235} fission induced by 14-Mev neutrons, although a clear separation of the two peaks was not observed.

The left-hand peak of the curves in Fig. 5 results from the existence of a bridge connecting the two hills of the W_{ik} surface. This bridge is absent in the spontaneous fission of Cf^{252} and slow-neutron fission of U^{235}, but appears with increasing energy of the neutrons that induce U^{235} fission. Fission in which the points of the W_{ik} surface are on the bridge is often called symmetric. We note, however, that not only actually symmetric fission, but many asymmetric fissions are represented by points near the bridge.

Figure 6 shows the total number of fission events corresponding to vertical slices of $\Sigma E = const$ at 3-Mev intervals. The most probable value, ΣE_{pr}, was 150 Mev. It is interesting that the bridge on the W_{ik} surface is most pronounced for $\Sigma E < \Sigma E_{pr}$.

We shall now consider the total number of

FIG. 6. Total fragment energy from photofission of U²³⁸.

FIG. 7. U²³⁸ photofission fragment energy E_1 measured with a single chamber. The dashed curves represent light and heavy fragment energies measured separately by means of two chambers.

FIG. 8. U²³⁸ photofission fragment energy E_1 in one chamber for three different intervals of total fragment energy: a— $105 < \Sigma E < 135$ Mev; b— $135 < \Sigma E < 165$ Mev; c— $165 < \Sigma E < 195$ Mev.

fissions as a function of E_1 for E_2 = const at 1.5 -Mev intervals (Fig. 7). This corresponds to the measurement of fragment energies in only one of the two chambers. The dashed curves in Fig. 7 represent the energy distributions of heavy and light fragments as determined by means of both chambers. Our curves are in satisfactory agreement with reference 3 when a correction for target absorption is introduced, but differ considerably from reference 2.

Our data also provided us with the energy spectra of fragments for three intervals of ΣE (Fig. 8). It is here seen that the valley between the peaks in Fig. 7 does not characterize symmetric fission, because each ordinate in Fig. 7 is the sum of the corresponding ordinates for the three curves in Fig. 8, and a peak of the curve in Fig. 8c almost coincides with valleys of curves a and b.

In conclusion, we present a summary of the quantities that usually characterize the energy distribution of fission fragments. The authors
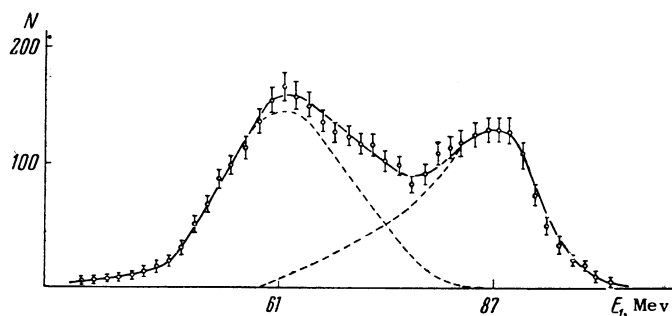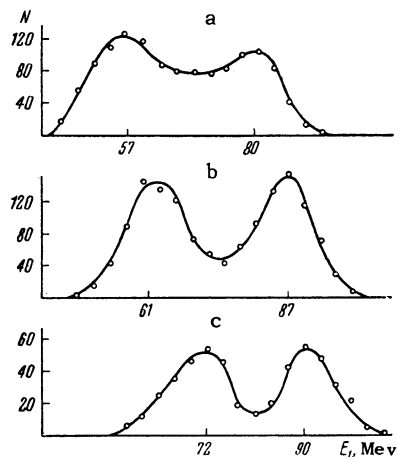
wish to thank the synchrotron team of the Physico-Technical Institute for the uninterrupted operation of the synchrotron, and Yu. Morozov and B. K. Gormin for technical assistance.

[1] L. E. Lazareva and N. V. Nikitina, Физика деления атомных ядер,(The Physics of Atomic Fission), Atomizdat, 1957, p. 189.

[2] Korotkova, Cherenkov, and Chuvilo, Doklady Akad. Nauk SSSR 106, 811 (1956), Soviet Phys.-Doklady 1, 104 (1956).

[3] Kovrigin, Kondrat'ko, and Petrzhak, JETP 36, 315 (1959), Soviet Phys. JETP 9, 217 (1959).

No.	Experimental quantities	Uncorrected	Corrected for source thickness	Correction for ionization defect
1	Most probable light-fragment energy, Mev	87±1	91.5±1	+5.6
2	Most probable heavy-fragment energy, Mev	61±1	64.5±1	+6.8
3	Ratio of most probable energies	1.43±0.04	1.42±0.04	
4	Most probable mass ratio	1.36±0.04	1.36±0.04	
5	Half-width of high-energy peak, Mev	17		
6	Half-width of low-energy peak, Mev	19		
7	Valley-to-peak ratio for high-energy peak	0.7		
8	Most probable total (kinetic) energy ΣE, Mev	150±2	157.5±2	+12.4
9	Half-width of total energy peak, Mev	31		

[4] R. B. Leachman, International Conference on the Peaceful Uses of Atomic Energy, Geneva, August 1955, Vol. 2, Russ. Transl. Goztekhizdat 1958, p. 220.

[5] W. Jentschke and F. Prankl, Z. Phys. **119**, 696 (1942).

[6] D. C. Brunton and G. C. Hanna, Can. J. Research **28A**, 190 (1950).

[7] D. C. Brunton and W. D. Thompson, Can. J. Research **28A**, 498 (1950).

[8] Smith, Friedman, and Fields, Phys. Rev. **106**, 779 (1957)

[9] I. V. Chuvilo, Dissertation, Physico-Technical Inst., Acad. Sci. USSR, 1952.

[10] Katz, Kavanagh, Cameron, Bailey, and Spinks, Phys. Rev. **99**, 98 (1955).

[11] Smith, Friedman, and Fields, Phys. Rev. **102**, 813 (1956).

[12] J. S. Wahl, Phys. Rev. **95**, 126 (1954).

[13] Bogachov, Vorob'ev, and Komar, Izv. Akad. Nauk SSSR, Ser. Fiz., **20**, 1455 (1956), Columbia Tech. Transl. p. 1331.

Translated by I. Emin

268